THESIS FOR THE DEGREE OF LICENTIATE OF ENGINEERING

Weldability and Testing Methodology in Precipitation Hardening Superalloys

JONNY JACOBSSON

Department of Industry and Materials Science

CHALMERS UNIVERSITY OF TECHNOLOGY

Gothenburg, Sweden 2017

Weldability and Testing Methodology in Precipitation Hardening Superalloys

JONNY JACOBSSON

Technical report no IMS-2017-5

Department of Industry and Materials Science
Chalmers University of Technology
SE-412 96 Gothenburg
Sweden
Telephone + 46 (0)31-772 1000

Cover:
Varestraint test plate (Haynes 282) with penetrant fluid under UV-light revealing solidification and liquation cracks, see DOE study page 14 for how the result can be used.

Printed and bound by Chalmers Reproservice
Gothenburg, Sweden 2017

Weldability and Testing Methodology in Precipitation Hardening Superalloys

JONNY JACOBSSON

Department of Industry and Materials Science
Chalmers University of Technology

Abstract

Usable weldability data is desired in the manufacturing industry, especially within the aerospace industry where fabrication of structural jet engine components are realized. Welding of precipitation hardening superalloys such as Waspaloy®, Alloy 718, ATI® 718Plus™ and Haynes® 282® in particular can lead to solidification cracking in the fusion zone, liquation cracking in the heat affected zone and/or to solid state cracking. This concern requires some kind of weldability testing such as Varestraint testing to improve the fundamental knowledge on how to prevent this type of cracks from occurring. It was found that the micro-hardness for all four alloys is approximately 250HV in the weld metal while the parent metal differs more, 208HV for Haynes® 282®, 243HV for Alloy 718, 340HV for Waspaloy® and 384HV for ATI® 718Plus™. The hardness in the HAZ reaches about 400HV for Waspaloy® and ATI® 718Plus™, while Alloy 718 and Haynes® 282®approach 250-350HV. The grain size is smallest for ATI® 718Plus™ (8.3 µm) and Alloy 718 (16µm) followed by Haynes® 282® (64µm) and Waspaloy® (90µm). Simulation using JMatPro suggested a larger amount of γ' in ATI® 718Plus™ compared to Alloy 718. In Haynes® 282®, the sigma-phase and M_6C levels are higher compared with those in Waspaloy®, for which $M_{23}C_6$ was found instead. Based on measurements, system analyses and design of experiment it was concluded that the lowest variation in evaluating weld cracking can be achieved with the method using penetrant combined with the use of one operator. The welding speed affected the variation in weld cracking most followed by current, die mandrel radius and the bending stroke rate. Testing parameters with lowest standard deviation/mean Total Cracking Length (TCL)-values are here found for welding speed of 1mm/s, weld current of 70A, die mandrel radius of 60mm and bending stroke rate of 10mm/s. The compression strains in the lower part of the specimen during the bending at Varestraint testing have no significant impact on the weld cracking. Based on Varestraint testing of Alloy 718 and Waspaloy®, there was similar cracking response at 1.1% to 4.3% augmented strain and if extrapolated downwards the critical strain from crack initiation approach zero. Similar to Alloy 718 and Waspaloy®, it was also found that ATI® 718Plus™ and Haynes® 282® both seemed to have a level of critical augmented strain of around 1% while at the highest strain level of 8.6% Haynes® 282® showed somewhat higher susceptibility values. The lower susceptibility to hot cracking in ATI® 718Plus™ compared to Alloy 718 and Haynes® 282® is supposed to be associated with the smaller grain size of ATI® 718Plus™ despite of its higher hardness. The HAZ liquation cracking in Haynes® 282® seems to be connected to Ti-Mo based MC-type carbides.

Keywords: Weldability, Superalloys, Varestraint, Waspaloy®, Alloy 718, ATI® 718Plus™ and Haynes® 282®

Preface

This licentiate report is based on work performed at Industrial and Materials Science (Chalmers University of Technology, Gothenburg) and at the Research & Technology department (GKN Aerospace Engine Systems, Trollhättan).

Paper I **A Historical perspective on Varestraint testing and the importance of testing parameters**
Joel Andersson, Jonny Jacobsson and Carl Lundin
Conference Paper, 4th International Hot Cracking Workshop, Berlin, Germany, April 2014.

Paper II **Improved understanding of Varestraint Testing - Nickel-based superalloys**
Joel Andersson, Jonny Jacobsson, Anssi Brederholm and Hannu Hänninen
Conference Paper, 4th International Hot Cracking Workshop, Berlin, Germany, April 2014.

Paper III **Weldability of Ni-Based Superalloys Waspaloy® and Haynes® 282® - A study performed with Varestraint testing**
Jonny Jacobsson, Joel Andersson, Anssi Brederholm and Hannu Hänninen
Research & Reviews: Journal of Material Sciences, 4 (4), 2016, pp. 3-11.

Paper IV **Weldability of Superalloy 718 and ATI® 718Plus™ - A study performed with Varestraint Testing**
Jonny Jacobsson, Joel Andersson, Anssi Brederholm and Hannu Hänninen
Materials Testing, 59 (9), 2017, pp. 769-773.

Contents

Introduction

The invention of airplane began in the 16th centuries with the first serious attempt on research into aerodynamics – the study of the forces operating on a solid body e.g. in a stream of air. Leonardo da Vinci and Galileo Galilei in Italy, Christiaan Huygens in Netherlands and Isaac Newton in England all contributed to an understanding of the relationship between resistance (drag) and e.g. surface area to the stream and the density of a fluid. When it comes to the first flight the successful airship (159kg steam engine 2.2kW, 44 meters hydrogen bag) by Henri Giffard of France in 1852 was flown at a speed of 10km per hour to cover a distance of about 30km. The invention of the airplane is referred to the evening of Sep. 18, 1901 when a 33-year-old businessman from Dayton, Ohio in United States of America, addressed a distinguished group of Chicago engineers on the subject of "Some Aeronautical Experiments" that he had conducted with his brother Orville Wright for the previous two years. He pointed out three general classes of difficulties, namely sustaining wings, power generation and balancing & steering. The first fully controllable and practical airplane (heavier-than-air craft) is therefore considered to be Wright flyer of 1905, third powered airplane designed, built and flown by Willbur and Orville Wright. It was powered by a four-cylinder engine (15-16kW) and the pilot lay prone on the lower wing with a hand lever to directly control the vertical rudder at the rear of the craft. [1]

The word *turbine* has a Latin root, *turbare*, which means *to stir up* and was invented circa 1837 by Professor Claude Burdin (1790-1873) to refer to water wheels converting hydraulic energy into useful horsepower. A water turbine about 0.3 m in diameter developed by one of his students, Benoît Fourneyron, produced 60 hp, which emphasize the of potential of turbines as an economically attractive approach to higher power levels compared to the piston engines with practical-economical size limits. The transition to gas turbines started in early 1941 during the world war two with the PT1 (Propeller Turbine no. 1) *free-piston compressor* which principally is a supercharged two-stroke diesel cycle. However, the traditional turbine look came with PT2 which started in 1945 and continued for fifteen years [2].

The jet engine started off as a military engine and after about a quarter of a million of service-hours it was offered as a commercial engine. This practice came from the piston engine era and continued up through the introduction of turbofans when the design of military and commercial engines moved in different directions, namely high speed aircrafts in the military and below Mach 1 for commercial aviation. Also, the development of power output kept climbing for the commercial jet engines while the military engines leveled off around 80 kN of thrust [2].

Specific fuel consumption (SFC) is a driving force for higher efficiency through increased turbine entry temperature (TET) where materials and manufacturing development have led to higher performance in the jet engine components. The turbine blade has changed to be internally cooled in early 1960s followed by thermal barrier coatings in late 1990s. The material has gone from wrought material to conventional cast in the mid-1950s over to directionally solidified cast alloys in 1970s followed by single crystal cast alloys in the 1980s. The surrounding components have therefore been forced to follow the increasing temperature trend. Today, in production of hot structural components, a fabrication strategy is being utilized where combinations of wrought, cast and/or sheet material with their different

properties are joined together by welding into large structural components. This put demands into the understanding of joining and welding processes when typically 60m of welds and segments are bonded through specific thermo-cycles. Weld repairs may also be needed either because of interruptions or defects related to service conditions [3].

The aim of this work has been to investigate weldability and testing methodology using already established and also newly developed precipitation hardening Nickel- and Nickel-Iron-based superalloys.

The research objectives in this research have to been to:

- Investigate the robustness in terms of repeatability of the Varestraint test as an evaluation method for weldability, with special emphasis on:
    - Welding parameters
    - Fixturing setup
- Investigate the hot cracking susceptibility in sheet form of Alloy 718, Haynes 282, ATI 718Plus and Waspaloy with special emphasis on grain size and hardness

Scientific and industrial contribution

The published weldability data can be used and further elaborated on in order to improve models for weld simulation where the risk for cracking can be determined. The Varestraint crack evaluation method using fluorescent penetrant inspection for crack measurements can be a valuable procedure to utilize since it lowers the risk of person-to-person interference.

It should also be emphasized that a more efficient production with less disturbances and repair work is the main goal for the industry. This is reachable if severe weld defects like hot cracks could be avoided.

Superalloys

Generally, superalloys can be divided into four categories depending on the matrix element(s), namely Iron-base, Nickel-Iron base, Nickel-base or Cobalt-base. These super-performing alloys at elevated temperatures (above 0.6 T_m) with maintained strength in corrosive environment through fatigue cycling are used in several different areas including the power generating and the aerospace industry. When looking at the weldability point of view, four alloys [4–7] of interest are selected as follows. These are Waspaloy® (early 1950´s), Alloy 718 (late 1950´s), ATI® 718Plus™(early 2000´s) and Haynes® 282®(mid 2000´s) with a service temperature of up to around ~750°C, ~650°C, ~700°C and ~800°C, respectively. These alloys are all so-called precipitation strengthened superalloys and contain additions of Titanium, Aluminum and/or Niobium that form strengthening precipitates with Nickel after appropriate heat treatment. These precipitates are mostly coherent with the austenitic matrix causing substantial increase in strength due to lattice strain effects [8].

Microstructural properties

The different phases found in superalloys besides the austenitic matrix range from larger trans- and intergranular carbides via the strengthening precipitates to small complex borides. The interphase between in particular the strengthening precipitates and the matrix determine the coherency and the desired hardening effect.

Gamma matrix (γ)

The wanted structure in the gamma matrix, γ, is the most closely packed FCC (face centered cubic) crystal structure. This structure means low diffusivity, possible phase stability from zero to melting point and common enough to be economical. It is usually based on Nickel with high percentage of solution hardening elements like Cobalt, Chromium, Molybdenum, Iron and Tungsten, to repel the overall decreasing strength with increased temperature.

Gamma prime (γ')

This phase has also a FCC structure, which is ordered, coherent with the matrix and appears in precipitates uniformly through the matrix. The nominal composition is $Ni_3(Al,Ti)$ and other elements that can participate in the precipitate include Niobium and Chromium. The γ' phase contributes to the high temperature strength and creep resistance of superalloys owing to the increasing yield strength with temperature up to ∼800°C. This effect is explained by ordering effects and relatively low mobility of so-called super dislocations [3]. The low mismatch, usually less than one percent, leads to slow coarsening rates of the precipitates [9].

Gamma double prime (γ'')

The gamma double prime, γ'', is coherent with matrix and have an ordered BCT (body centered tetragonal) unit cell with the nominal composition of Ni_3Nb. Also, the phase is more stable than the γ' due to large mismatch. This fact can be used for significant strengthening, but with the limitation to intermediate temperatures as for e.g. Alloy 718 where γ'' is precipitated besides some γ'.

Delta (δ) and Topologically Close-Packed (TCP) phases

The Delta phase, δ, has an orthorhombic structure and has nominally the same composition as the γ'' phase, Ni_3Nb. It is thermodynamically stable, incoherent with matrix and the contribution to strength is therefore very small. The plate shaped precipitation usually occurs at grain boundaries were prevention of grain growth is possible up to a point when the phase dissolves. The Topologically Close-Packed (TCP) phases (Laves, σ, μ) are undesirable, brittle and usually form during casting, heat treatments, welding or long time service.

Carbides

The most common metal carbides found in nickel based superalloys prefer grain boundaries as precipitation sites and are recognized as MC, $M_{23}C_6$, and M_6C. The carbides can have different kind of effect in the alloy, i.e. to inhibit grain growth, strengthen the alloy and also initiate fracture. The MC-type carbides have a FCC crystal structure and forms typically at the end of solidification by eutectic-type reactions with γ matrix. These MC-carbides can often be replaced by $M_{23}C_6$ and M_6C carbides during thermal processing and/or during service. The latter carbides have a complex cubic structure and the $M_{23}C_6$ carbides are generally rich in Chromium and form in the range 760-980°C. The M_6C carbides form in the range 815-980°C (Note Figure 11a) and usually form when the Mo and/or W content is greater than 6-8 at% [9].

Grain boundaries

In Nickel base weld metal there are at least three types of boundaries or interfaces which can be observed in light optical microscope after polishing and etching. The first type called Solidification SubGrain Boundaries (SSGBs) represents the finest structure separating cells or dendrites with no or low angle boundaries. Secondly, Solidification Grain Boundaries (SGBs) are found at intersection of packets or groups of subgrains where high angle grain boundaries forms. Solidification cracking occurs almost always along these high angle grain boundaries [10, 11] probably due to presence of low melting liquid films. The third type called Migrated Grain Boundaries (MGBs) can in some situations form when the crystallographic component migrates away from the compositional component during i.e. reheating or multipass welding [9].

Minor elements

Boron, Carbon and Zirconium are often added for grain boundary strengthening when creep resistance is required. For welding this need to be balanced especially due to the deleterious effect for Boron on solidification and liquation cracking susceptibility. The Boron content is usually held at 0.001-0.005wt% while a Zirconium level up to ~0.04wt% can be tolerated if not combined with a high Boron level. When Sulphur is held at concentrations <0.001wt% instead of 0.020-0.040wt% additional Boron and Zirconium can be tolerated. Generally should Phosphorus and Sulfur be held as low as possible since they do not have any benefit for the alloy properties from cracking resistance point of view.

Welding

Welding is a manufacturing process, in the aerospace industry large savings can be made by utilizing fabrication. Instead of producing advanced engine parts with complex casting or machine them from forgings they are welded together from more simple pieces. However, since a substantial amount of welding is carried out there is often a high risk of cracking. Therefore, there is a need for determining materials weldability which within the scope of research presented here is defined as its ability to avoid cracking during and after welding.

Cracking mechanisms

The cracks occurring in or related to welds can be divided into different categories dependent on how they form and they can be studied from thermal, metallurgical or mechanical point of view.

Solidification cracking

First category involves the solidification cracking which may be the worst type because after initiation it can grow until the weld stops. It forms in the remaining liquid during the last stage of solidification in between growing dendrites or columns. Often the solidification range or brittle temperature range is pointed out to be closely connected to the cracking susceptibility [12].

Liquation cracking

A second category is the Heat Affected Zone (HAZ) or liquation cracks were liquid also is present at grain boundaries and secondary phases close to the fusion boundary. These cracks forms mainly due to two reasons, constitutional liquation of secondary phases and/or liquation of segregated melting point depressant elements. In both cases rapid heating is required to cause large enough temperature and compositional gradients for crack formation. Slow heating would on the other hand lead to dissolution of second phase constituents through solid state diffusion into the matrix and the material will be more homogenized [12].

Solid-state cracking

Other categories of cracking include e.g. ductility dip cracking and strain age cracking, which all occur in the fully solid state. At intermediate temperatures of approximately 0.5-0.8Tm the ductility dip cracking can occur in locations of grain boundary embrittlement. Strain age or reheat cracking on the other hand occurs during a post-weld heat treatment which is carried out to improve mechanical properties and relief residual stresses due to welding while homogenizing the precipitation strengthened microstructure [12, 13].

Weldability testing

A weldability test should provide enough information whether a real weld can be successfully made or not. The tests could therefore be divided into three main categories, (representative, externally loaded and simulative tests), depending on the complexity of the test and the desired output.

Self-restraint tests

Here the geometry of the specimen is designed to produce variable restraint in the weld and is used to induce cracking without any external load. The test can represent the actual welding and restraint

conditions but normally only provides simple results, that is, if cracks exist or not afterwards. Some examples [14] of these tests can be seen in Figure 1.

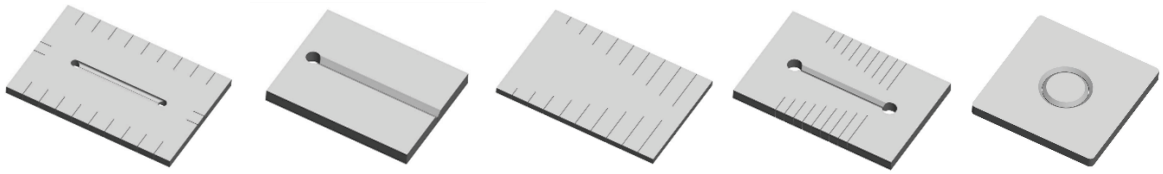

(a) (b) (c) (d) (e)

Figure 1. Illustrative examples of (a) Lehigh restraint test, (b) keyhole restraint cracking test, (c) Houldcroft crack susceptibility test, (d) keyhole slotted-plate restraint test and (e) circular patch test.

The **Lehigh restraint test** from Lehigh University uses a plate with slots of a specific length at the sides and ends to control the severity of the restraint. The test with a single-pass weld is repeated with different slot length until a threshold value is obtained.

Keyhole restraint cracking test from U.S. Naval Research Laboratory is a simplified version of the Lehigh test and uses a groove in the plate along the centerline and ends with a hole. A weld is made towards the hole where the restraint will reach a maximum and a crack may form. The length of the crack is measured and used as index for crack susceptibility.

The **Houldcroft crack susceptibility test** is similar to the Lehigh test but with varying slot length along the centerline and with a full penetration weld made. The restraint level is highest in the beginning of the weld and a mean value of crack lengths is used as susceptibility index.

Keyhole slotted-plate restraint test from Battelle is a variant of the Houldcroft test and begins at the low restraint end. The crack sensitivity is determined by the uncut width of the specimen at the point where the crack ends.

The **Circular Patch test** relay on the principle that stresses across the weld will increase along a circular path due to the shrinkage of the earlier weld. A centerline crack can initiate and grow along the path depending on thickness, diameter and weld parameters. The angle between starting and crack initiation point is used for susceptibility index.

Externally loaded tests

A second type of tests involve a load being applied externally either before or during welding in order to test the susceptibility to cracking. This is often done by measuring the load or the severity of the test at a level where cracks are initiated or arrested. A limitation for these tests is that the applied load is added to the shrinkage restraints making them difficult to separate, see Figure 2.

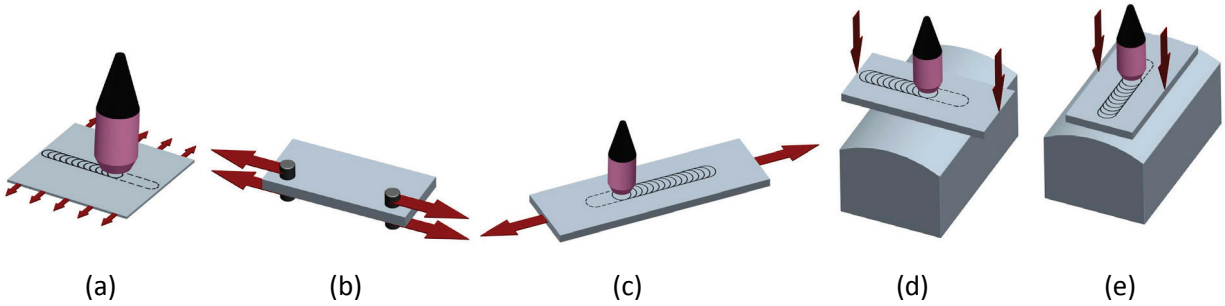

Figure 2. Illustrative examples of (a) Sigmajig, (b) Russell test, (c) PVR-test, (d) Varestraint test and (e) Transvarestraint test.

The **Sigmajig test** from Oak Ridge National Laboratory by M. Goodwin in 1987 [9] involves a sheet specimen which is transversely pre-stressed in a jig where a TIG-weld is then made along the centerline. The procedure is repeated with increased preload until cracking occur at the so-called threshold stress (σ_{th}). This works for thin sheet material up to approximately 2.5mm but a drawback supported with finite element calculation is found [15, 16] where the specimen can crack at stress-free condition and have no cracking at moderate pre-stress [17, 18].

Russell test by Derek Russell is a relatively simple test jig where a pre-strained test specimen is welded either to or from the high stress field. The load is measured with strain gauge and combined with the measured cracks which in general are found to become somewhat shorter when welding in the direction from the highest stress field. Advantages are the small size, ability to use relatively thick specimens and possibility to produce solidification cracks in even the most resistant steels while high scatter may require additional testing and use of mean values [19, 20].

The **PVR (Programmierter Verformungs-Riss)-test** also known as Controlled Deformation Cracking Test or Controlled Flat Tension Test was developed in Austria three decades ago. Here welding with constant speed is made on a flat tensile specimen while a constant accelerating strain rate is applied. The critical tension speed V_{cr} is used for susceptibility index at the first detected crack and it could be solidification cracks, liquation cracks or solid-state cracks. This can be done in one specimen and the procedure is internationally standardized [21] but the test requires high elongation to break which limits the suitable test material [12, 22].

The **Varestraint** from 1965 by Savage and Lundin [23] and **Transvarestraint test** from 1970 by McKeown [23] originates from “VAriable RESTRAINT” and “transverse” loading direction produces surface cracks usually by TIG-welding and bending a sample plate at the same time. This is done over pre-shaped die blocks often with hydraulic or pneumatic plunger and the applied strain is altered by changing die blocks. The tests are claimed to provide rapid testing and evaluation, low scatter and good reproducibility with the use of a single machine and the procedure are standardized [21]. The use of high strain rates is criticized [24] for potentially skewing the susceptibility results and for the fact that Transvarestraint testing only sheds light on solidification cracks.

Simulative tests

Simulative tests are tests where a defined weld temperature cycle is simulated and used to collect information in or near a crack susceptible location.

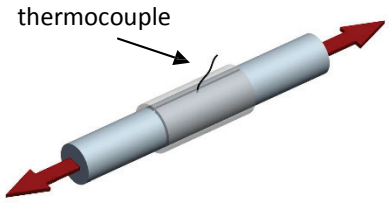

Figure 3. Illustrative example of Gleeble hot ductility test run above test material melt temperature.

The **Gleeble hot ductility test** from Rensselaer Polytechnic Institute in Troy is a method widely used and standardized [21] to measure material properties at high temperatures and can be used for studying solidification cracking where the material is heated above the melting temperature in a quartz tube, see Figure 3. Several specimens are broken at selected moments in the welding thermal cycle and the reduction in area is measured from fractured cross-section. Critical strain rate for crack initiation or ultimate fraction strength may be desired measurements [12, 25, 26].

Cast pin tear test is a relatively new test developed by Hull in the 1970´s and this test gives a minimum pin length for cracking to occur.

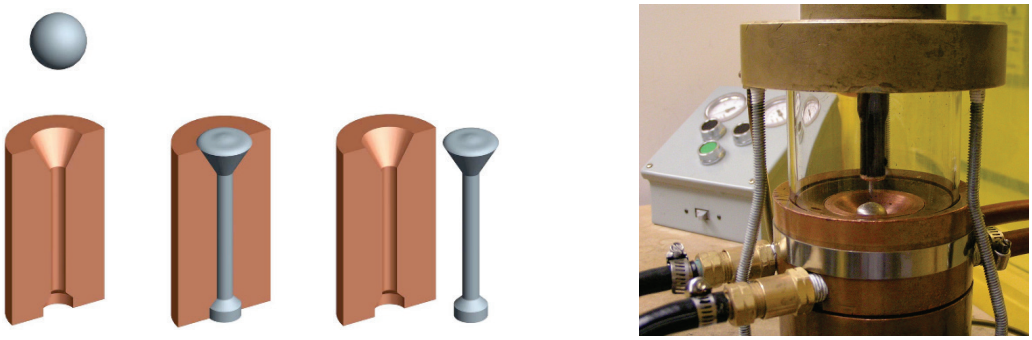

(a) (b)

Figure 4. Cast pin tear test in (a) illustrative example and (b) photo showing test setup [27] **.**

The small (typically 10-16g) test pieces are melted with a TIG equipment or an induction coil and then cast into Copper molds, Figure 4, of different length with help of gravity or small argon gas overpressure. The mold geometry and material behavior affect the tendency to form solidification cracks just below the pin head at a certain pin length [28].

Crack measurement and criteria

Cracks are generally reproduced in a test and then evaluated through measuring the cracks and important parameters and/or by counting the visible cracks. Often the measurements are done in the as-welded condition with the help of e.g. microscopy or penetrant inspection. In order to increase the reproducibility and lowering the manual error each specimen could be evaluated by two different

observers and then an average value is used or also the test could be repeated. A common measurement is the Total Crack Length (TCL) where all relevant cracks are measured and summarized while another measure, the Maximum Crack Length (MCL), only consider the longest crack and may be more sensitive to measuring errors. In addition, the similar Maximum Crack Distance (MCD) is defined as the perpendicular distance from the fusion boundary to the far-end tip of the crack and is identical at the centerline, see Figure 5a. The MCD is often combined with measurement of the thermal cycle to calculate the Brittle temperature range (BTR) or Solidification cracking temperature range (SCTR), Figure 5. Then it is also possible to use the total number of cracks or the point where the first crack is visible as indicator for hot cracking susceptibility.

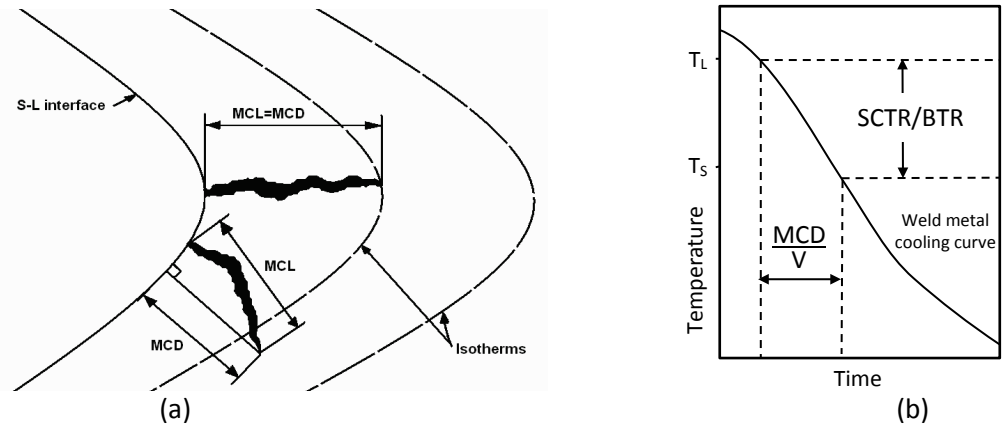

Figure 5. Principal (a) use of Maximum crack distance (MCD) and (b) comparison to Maximum crack length (MCL).

When trying to construct and find criteria for hot cracking, they are often based on the assumption that there exists a critical strain (CS). Depending on the type of test (i.e. bending or tension) and experimental conditions (i.e. sample geometries, thermal history, strain rate, etc.) the absolute value for the criteria can vary widely. A strain theory which combines both CS and critical strain rate (CST), Figure 6, defines the upper (TL) and lower temperature (TE) limits, while the critical ductility curve is determined experimentally, i.e. with a strain-based test. Cracking is assumed to occur when a deformation curve, representing strain across mushy zone, intersects the curve at any point [12].

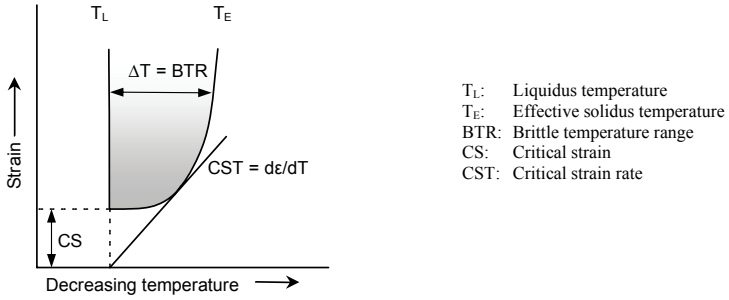

Figure 6. Schematic illustration of CS, CST and BTR in the ductility curve.

Experimental and Analyses Techniques

The experimental work in this study includes Varestraint testing and sample preparation (paper I, III and IV). The technique with fluorescence penetrant inspection combined with digital imaging was used in all four papers while microscopy and hardness measurements where done in papers III and IV. Additionally, JMatPro simulations where done in paper IV.

Material

The alloy compositions are summarized in Table 1 for the sheet materials used in the paper III and IV. These compositions are similar or identical as those in paper I and II. The Waspaloy® plates were solution-annealed at 1010°C for 2h followed by forced air cooling and Haynes® 282® is in mill-annealed condition (1121°C for 0.5h then polymer quench). Alloy 718 and ATI® 718Plus™ were solution-annealed at 954°C for 1h in paper IV while ATI® 718Plus™ was in mill-annealed condition in paper II.

Table 1 Specified alloy compositions in wt.%

Element wt%	Ni	Cr	Fe	Co	Mo	Al	Ti	Nb	C	P	B	W	Cu	Mn	S	Si
Waspaloy®	Bal.	19.13	1.13	13.34	4.22	1.36	3.03		0.08	0.004	0.006		0.02	0.02	0.002	0.09
Alloy 718	Bal.	18.41	17.92	-	3.05	0.60	0.94	5.00	0.03		0.002	-				
ATI® 718Plus™	Bal.	17.86	9.59	8.97	2.70	1.49	0.76	5.49	0.024		0.004	0.99				
Haynes® 282®	Bal.	19.63	0.35	10.35	8.56	1.41	2.21		0.068	0.002	0.004		-	0.08	0.002	-

Microstructure

The grain size in the different alloys studied in paper III and IV can be seen in Figure 7a-d. The smaller grain sizes were shown for ATI® 718Plus™ (8µm) and Alloy 718 (16µm) followed by Haynes® 282® (64µm) and Waspaloy® (90µm). The macro-hardness was measured to 367HV (solution-annealed), 227HV (solution-annealed), 204HV (mill-annealed) and 294HV (solution-annealed), respectively. The difference between macro- and micro-hardness levels in the different alloys were all within 16% which is not unexpected.

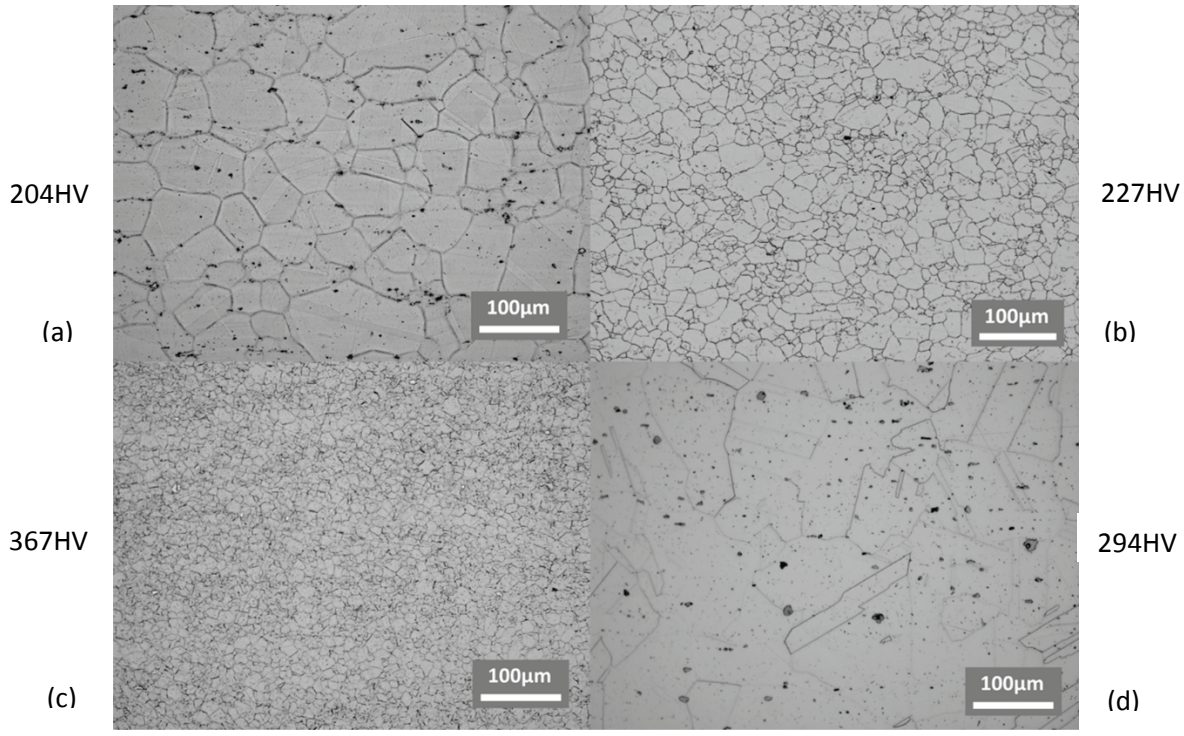

Figure 7. Wrought material in (a) Haynes® 282®, (b) Alloy 718, (c) ATI® 718Plus™ and (d) Waspaloy®.

In Figure 8 the Vickers micro-hardness variation can be seen across the weld for the different alloys studied in paper III and IV among the mean values for parent metal (horizontal straight dotted lines). The same hardness (250HV) is roughly found in the weld metal for all the measured alloys independent of the parent metal hardness. Highest values (around 400HV) are seen for Waspaloy® and ATI® 718Plus™ in the heat affected zone (HAZ) while the other alloys reaches about 250-350HV.

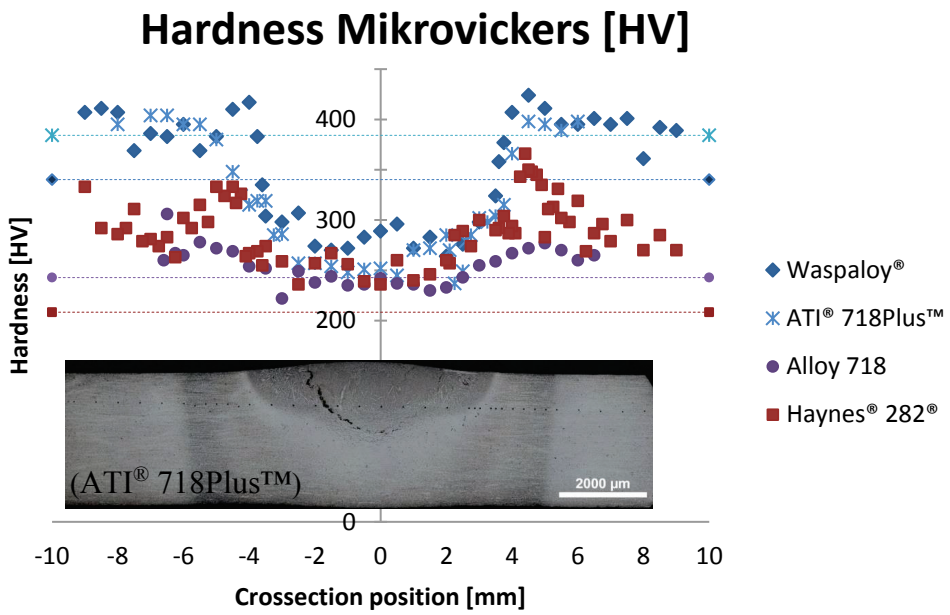

Figure 8. Micro Vickers hardness across weld section together with parent material values.

In the HAZ a similarity is found for Alloy 718 and Haynes® 282® were the hardness level reaches approximately 300HV. The main explanation to the differences in parent metal hardness for ATI® 718Plus™ (384HV, solution-annealed) is related to fast hardening of the γ' phase and for Waspaloy® (340HV, solution-annealed) associated with slow forced air cooling. Alloy 718 (243HV, solution-annealed) rule under sluggish hardening of the γ'' phase whereas Haynes® 282® (208HV, mill-annealed) undergoes a fast polymer quench.

Equipment

For some of the testing the relatively newly developed [29] Varestraint machine, Figure 9, at University West in Trollhättan Sweden was used where the designed capacity is 100 ton in the press at stroke rates up to 350 mm/s (due to the pressurized accumulator tanks) with a good stop position accuracy capable of 65 ms in response time. Several different test modes apart from Varestraint testing can be used including Transvarestraint, Spot Varestraint, multi-pass testing, bending without welding and filler material studies.

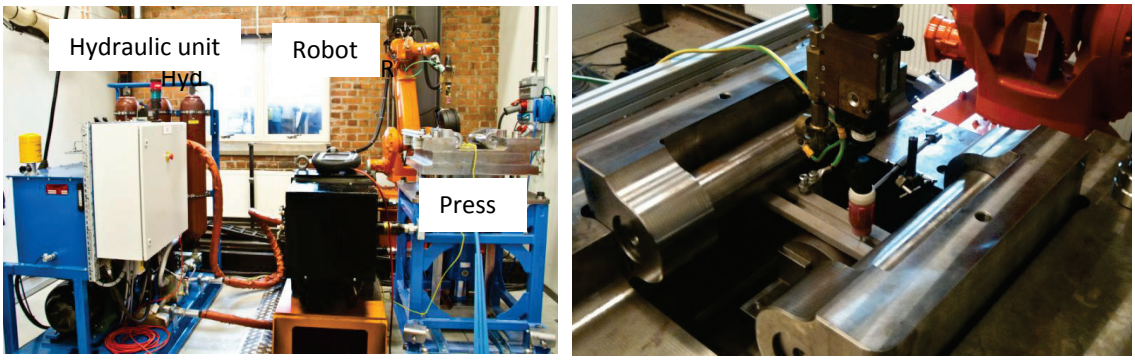

(a) (b)

Figure 9. Varestraint test equipment including (a) hydraulic unit, welding robot and (b) press.

Simulation

The amount of γ' and γ'' hardening phases could be visualized or thought of as one weldability affecting parameter where Waspaloy® followed by ATI® 718Plus™, Haynes® 282® and Alloy 718 are shown in descending hot cracking susceptibility ranking due to the associated restraining effect from the hardening phases, Figure 10a. When looking at other present phases in Alloy 718 and ATI® 718Plus™ the result is more or less identical as in Figure 10b, that is, MC-formation at 1250°C followed by Delta and mostly Laves which can start to form roughly at below 1150°C.

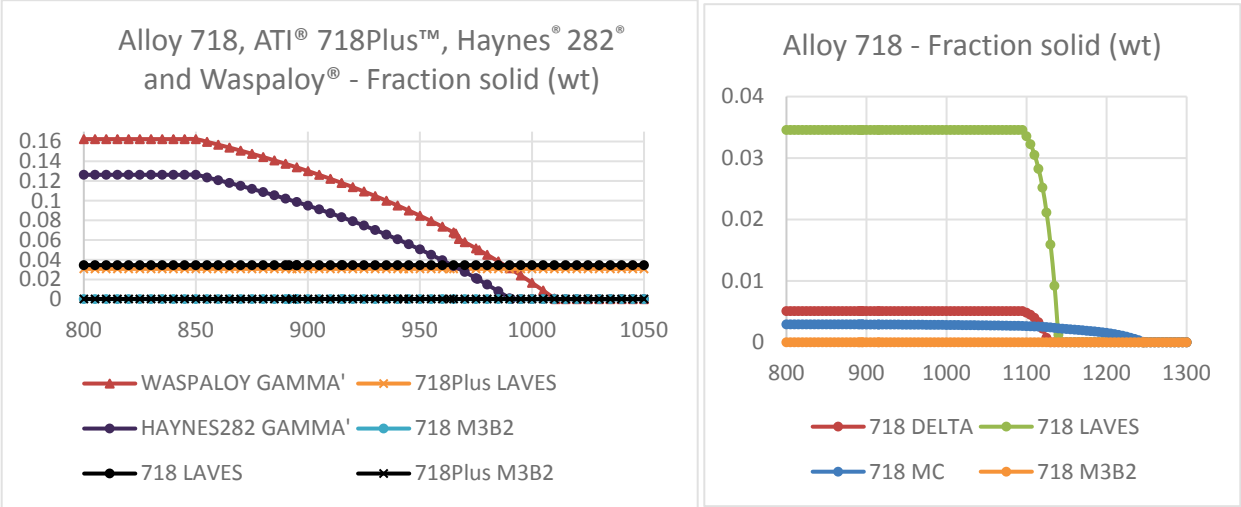

Figure 10. (a) Solidification weight fraction of γ' and γ'' in JMatPro and (b) Alloy 718 phases.

For Haynes® 282® and Waspaloy® the solidification sequences are different, Figure 11, for example the amount of sigma-phase is smaller in the latter material. Then, M_6C is present in Haynes® 282® while instead $M_{23}C_6$ is found in Waspaloy®. Note that M_6C can start to form around 1250°C according to this simulation.

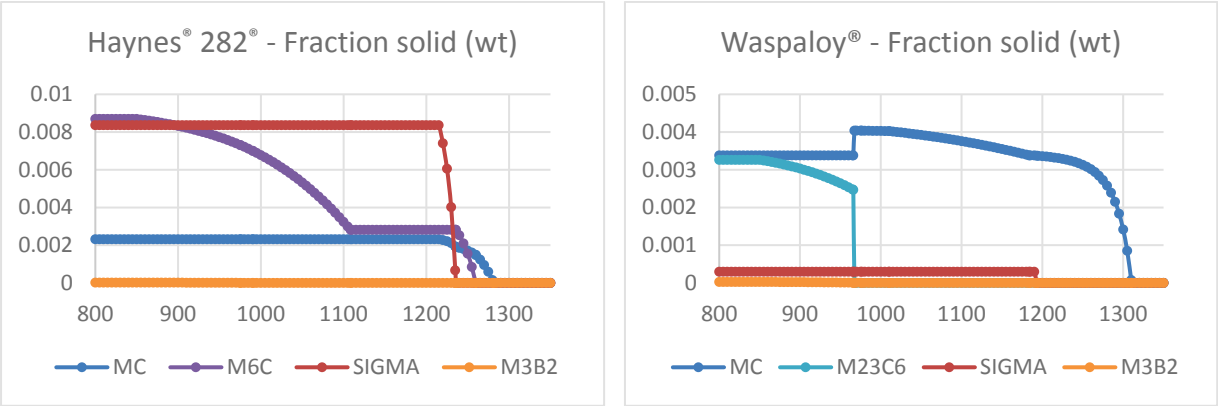

Figure 11. Solidification weight fractions of phases with JMatPro in (a) Haynes® 282® and (b) Waspaloy®.

Summary of results in appended papers

A distinction must be made regarding the Varestraint test results in Paper III, it is not directly comparable with the results in Paper I due to the use of different test equipment and to the lack of similarity in the chosen test parameters. This problem has been studied earlier in a round-robin study [22] and also in the work on how to standardize the test procedure [24].

Paper I

In this study, the influencing weldability parameters around the new Varestraint machine are evaluated through Measurement System Analysis (MSA) and Design of Experiment (DoE). The MSA showed that the penetrant evaluation method had a relatively low variation compared to the microscopy method due to the repeatability. Also, the use of one operator would reduce the variation in both methods due to consequential judging and in this case 28% of the natural variation is due to the measurement system (penetrant method with one operator). The DoE consisted of 4 test parameters with 3 repetitions each and 10 center points in a 2^{nd}-level full factorial experiment. In a main effect plot, Figure 12, the blue line represents the standard deviation divided by the mean value which should be minimized in order to have a small influence from the measurement system. Best parameters to use should have a low std-dev/mean combined with a variation below the mean value (black horizontal line) which is the case for the parameter in Figure 12b where the two best settings are highlighted and the other are adequate alternatives.

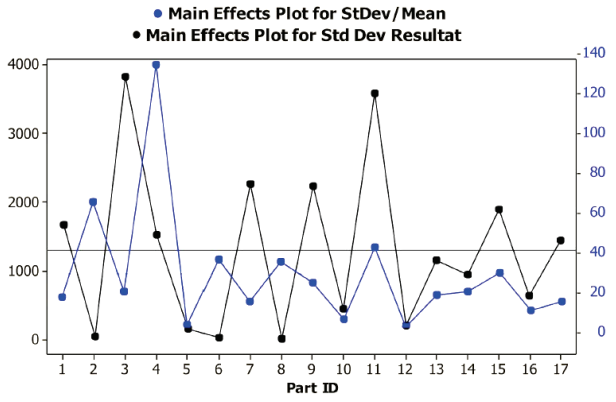

(a)

Parameter setting	5	10	12	13	14	16	17
Weld Speed (mm/s)	1	3	3	1	3	3	2
Weld current (A)	70	70	90	70	70	90	80
Radius (mm)	60	40	40	60	60	60	50
Stroke rate (mm/s)	10	250	250	250	250	250	130
Stdev	145	437	206	1147	940	638	1447
Stdev/mean (%)	3	6	2	18	20	10	15

(b)

Figure 12. DoE results with (a) main effect plot of mean std-dev and normalized values and (b) selected parameters sets.

In an interaction plot, Figure 13, it is visible that the stroke rate (speed of impact) has relatively low effect on the variation while weld speed affect most. The lowest variation is achieved with low welding speed, current, stroke rate and large radius but this setup could lead to zero or very few cracks to measure which may not be practically desired.

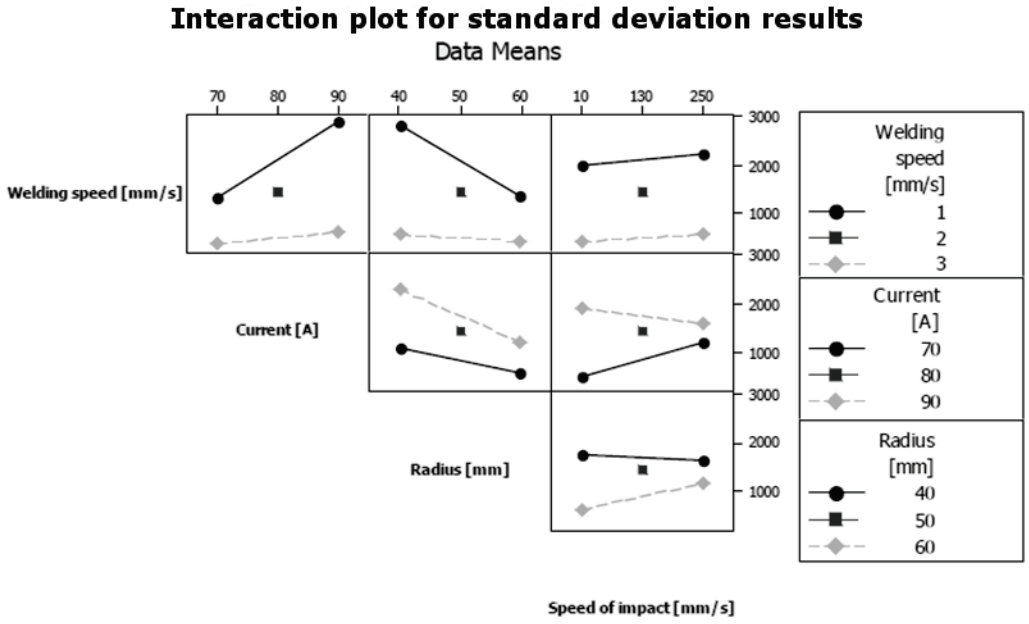

Figure 13. Interaction between input parameters on the variation in total crack length.

Conclusions (paper I)

- One operator results in less variation in reproducibility due to the subjectivity of the measurement procedure and lack of training.
- The welding speed is according to the DoE the cause for the greatest variation.
- Low standard deviation/mean-TCL are found for the parameters: welding speed of 1mm/s, weld current of 70A, radius of 60mm, bending rate of 10mm/s)
- Measurements should be performed on samples with TCL above ~9.4mm which stand for a measurement variation of ~28 %.

Paper II

In this paper, a study is carried out in relation to the suggestion to use test plates thicker than 10 mm to avoid hinging and in order to minimize the influence of the compression strains (lower part of the bent specimen) on the weld cracking during bending. This is done in Varestraint testing on ATI® 718Plus™ and Haynes® 282® plates using test configurations with and without bottom-tack-welded support plates where the TCL response versus ideal augmented strain is considered. The test on ATI® 718Plus™, Figure 14, shows that no distinction between the different plate configurations could be made despite the presumably different strain situations.

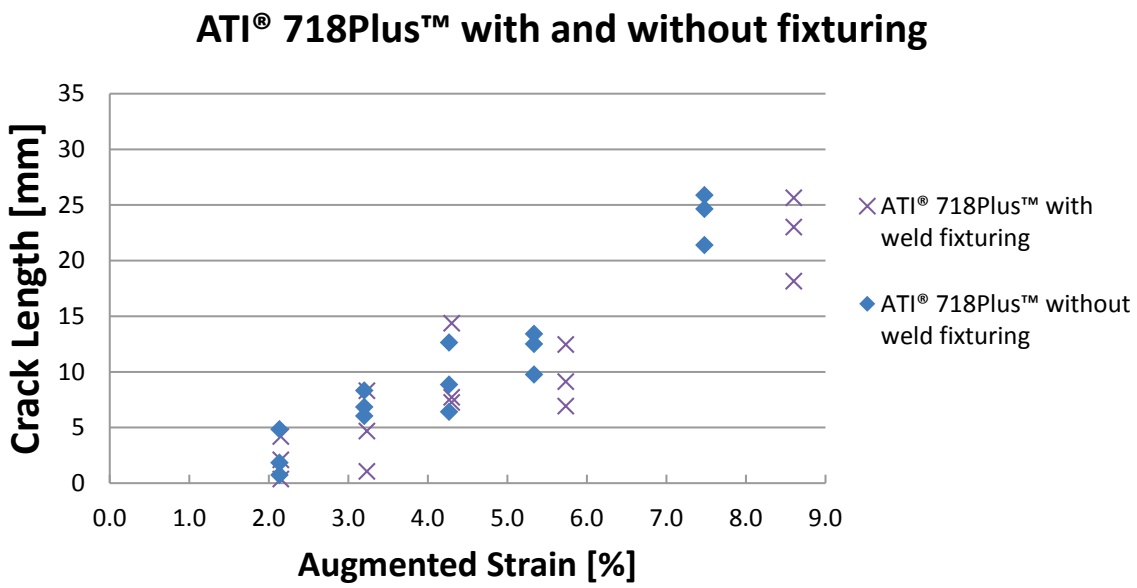

Figure 14. Varestraint test on ATI® 718Plus™ comparing with and without fixturing.

The results from the Haynes® 282® specimen, Figure 15, also show an insignificant difference concerning the use of fixturing and the negligible influence of the compressive state. It should be noted that the large difference in grain size (ASTM 5 for Haynes® 282® and very fine ASTM 10 for ATI® 718Plus™) can be expected to be an advantage for Haynes® 282® if grain size refinement is possible.

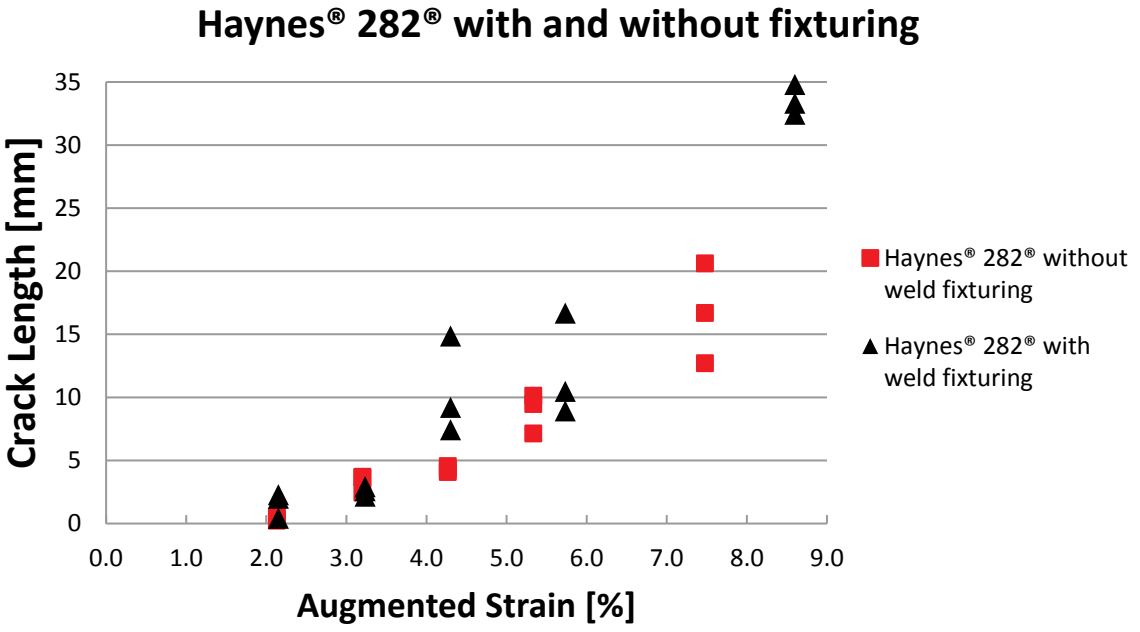

Figure 15. Varestraint test on Haynes® 282® comparing with and without fixturing.

Conclusions (paper II)

- No influence of the compressive strains on the cracking response in Varestraint testing was observed.
- Thin test plates can be used as long as kinking is eliminated by the use of support plates.
- Hot cracking susceptibility of Haynes® 282® is lower compared to that of ATI 718Plus® especially when the grain size effects are considered.
- ATI 718Plus® liquates through constitutional liquation of NbC.

Paper III and IV.

Varestraint test results can be seen in Figure 16. Varestraint test results in the form of TCL [mm] versus augmented strain [%], Figure 16, which show different similarities between the four studied alloys. Firstly, Alloy 718 and Waspaloy® tend to point towards zero tolerated augmented strain when looking in the tested range (1.1%-4.3%). Secondly, ATI® 718Plus™ and Haynes® A282® seems to have a tolerance of around 1% applied strain even if the highest values (8.6%) indicates somewhat higher values for the latter alloy. The test setup parameters included current of 85A, stroke rate of 16mm/s and weld speed of 2mm/s.

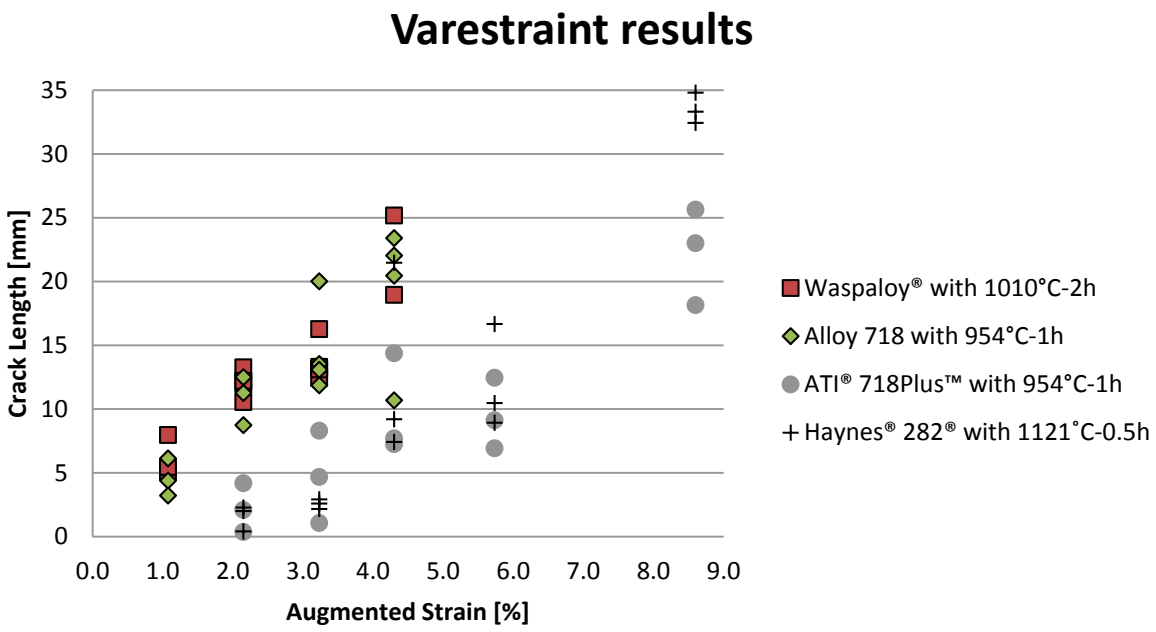

Figure 16. Varestraint test results in the form of TCL [mm] versus augmented strain [%].

Closer look on the Varestraint samples in the heat affected zone (HAZ) showed that there where intergranular liquation cracks, Figure 17a-d, but with different appearance in the four alloys. In Alloy 718 and ATI® 718Plus™ tested at strain level of 4.3%, along the crack paths and also ahead of the crack tips γ-

Laves eutectic is expected [30–33]. In the Haynes® 282® sample there are small amounts of traces from liquation which could be Ti-Mo based MC and/or M_5B_3 [13]. Waspaloy, on the other hand, showed no visible traces of liquation at this magnification, c.f. [34].

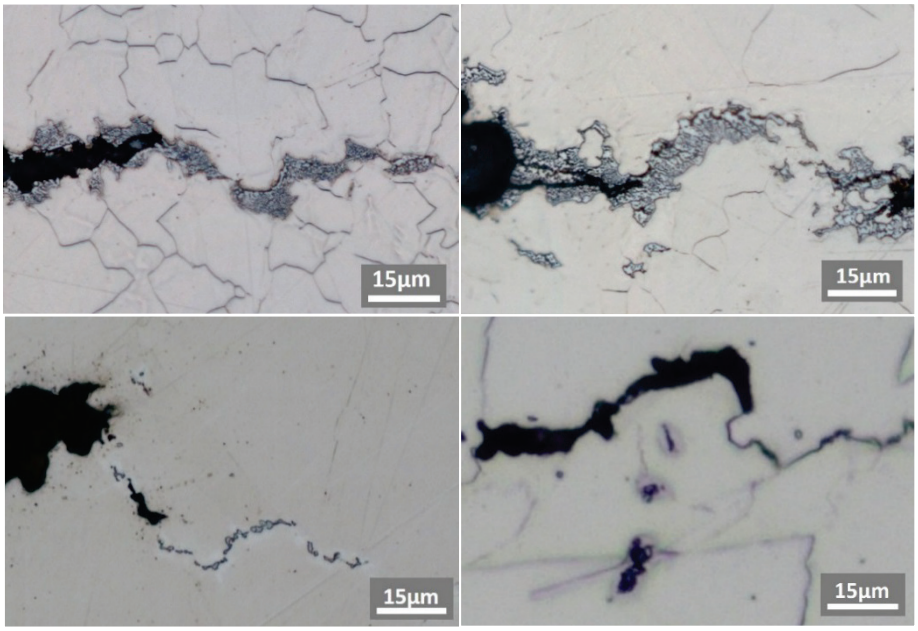

Figure 17. HAZ liquation and crack tip sections in (a) Alloy 718, (b) ATI® 718Plus™ (c) ™ Haynes® 282® (d) Waspaloy®.

Conclusions (paper III and IV)

- ATI® 718Plus™ showed lower susceptibility to hot cracking than Alloy 718 in Varestraint testing despite of its higher hardness, which was associated with the smaller grain size of the specific ATI® 718Plus™ material used in the current study.
- ATI® 718Plus™ and Alloy 718 reveal increased hot cracking susceptibility in their mill-annealed condition as compared to that of their solution-annealed condition (954°C for 1 h). The solution annealing lowers the hardness, but does not influence the grain size.
- The susceptibility to hot cracking is higher for Waspaloy® than for Haynes® 282® according to the Varestraint test and this is supported by the earlier testing on as-received Waspaloy® and Gleeble hot ductility tests.
- In Haynes® 282®, HAZ liquation cracking was connected to the presence of an intergranular secondary phase which seems to be similar to what was identified earlier in the FZ, namely Ti-Mo based MC-type FCC carbides.

Future work

In recent work, the old “Elegant version” of the Varestraint concept [23] seems now more realistic to be constructed and implemented as a complementary tool to the relatively new Varestraint machine at University West in Trollhättan Sweden, see Figure 18. If this approach works as expected solidification crack initiation could be captured in every sample at a relatively low strain rate. This could give new insight and/or confirmation of today’s test methods and procedures.

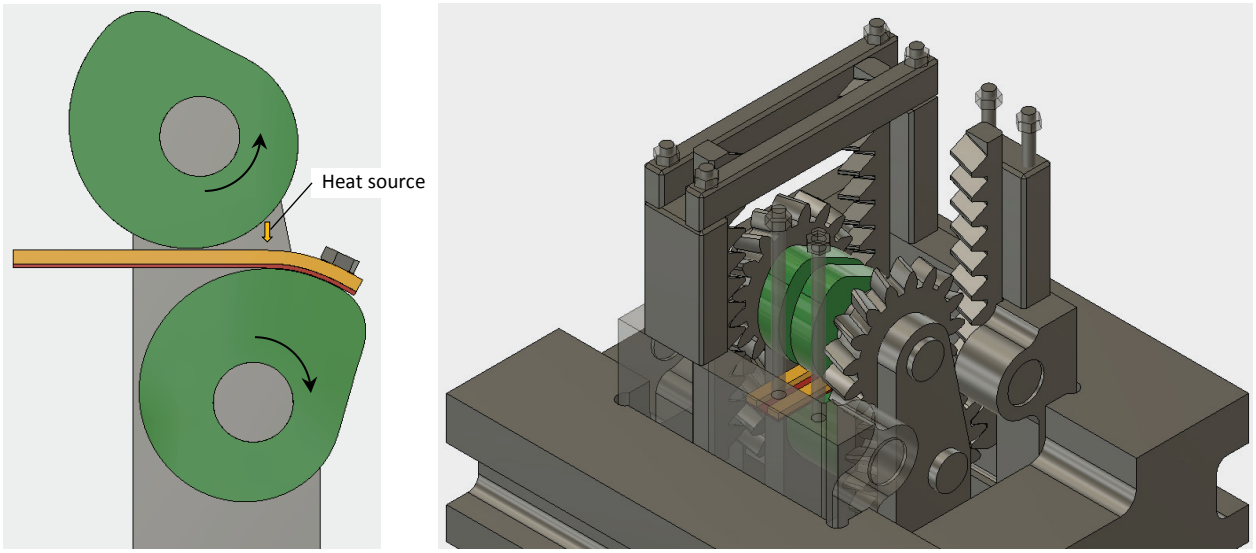

Figure 18. (a) Principle view and (b) overview of early concept model of a possible accessory in the Varestraint machine.

The modified machine is intended to have a pre-shaped upper pair of mandrels and a lower one rotating in the direction to bend the support and test plates against the lower mandrel where they are fastened. The mandrels are pre-shaped presumably with involute, in order to achieve increasing strain during welding locally near the weld pool. The radius of the mandrels and gears are maximized with the intention of enabling low minimum applied starting strain and at the same time allowing the use of the available piston movement. The gears can be helical or double-helical to get smooth movements and the racks are fastened to the piston grips. Roller bearings if any should be of needle type to handle the loads. Then, four supporting brackets are fastened in the press unit and two shafts with splines or grooves at the mandrels and gears transfer the moment from the gears to the mandrels. The welding heat source is placed between the two upper mandrels to balance the weld pool horizontally right in position to the deformation zone.

Acknowledgement

I want to thank my supervisor Assoc. Prof. Joel Andersson, retired supervisor Adj. Prof. Göran Sjöberg, examiner Prof. Lars Nyborg. The support by the Consortium Materials Technology for Thermal Energy Processes (KME) through funding from Swedish Energy Agency and GKN Aerospace Sweden AB is highly appreciated. Mr. Bengt Johansson at GKN Aerospace Sweden AB is especially acknowledged for his support in performing some of the heat treatments and of course a lot of people helping out with the work i.e. milling, wire EDM and robot programming.

References

[1] Crouch, T.D., History of flight. *Academic.eb.com.proxy.lib.chalmers.se/levels/collegiate/article/history-of-flight/390563* 2017, Britannica ACADEMIC.

[2] Connors, J., The Engines of Pratt & Whitney A Technical History, American Institute of Aeronautics and Astronautics, Inc., 2010.

[3] Reed, R.C., The Superalloys - Fundamentals and Applications, University Press, Cambridge, 2006.

[4] Thielemann, R.H., Mertz, J.C., Eddy, W.P.J., Trends in gas turbine engine materials, in: *SAE Annual Meeting, Hotel Book-Cadillac, Detroit, Michigan January 14-18*, SAE inc., 1952, p. 14.

[5] Haynes international, HAYNES ® 282 ® alloy. *Http://haynesintl.com/alloys/alloy-portfolio_/High-Temperature-Alloys/HAYNES282alloy/principal-features_copy1.aspx* 2017.

[6] Eiselstei, H.L., Age-hardenable nickel alloys, US3,046,108, 1962.

[7] Ott, E. a., Groh, J., Sizek, H., Metals Affordability Initiative: Application of Allvac Alloy 718Plus for Aircraft Engine Static Structural Components. *Superalloys 718, 625, 706 Var. Deriv.* 2005, 35–45.

[8] Rao, M.N., WROUGHT SUPERALLOYS – SCIENCE, TECHNOLOGY AND APPLICATIONS, in: Watson, J.E. (Ed.), *Superalloys: Production, Properties…*, Nova Science Publishers, Inc., 2011, pp. 25–43.

[9] DUPont, J.N., Lippold, J.C., Kiser, S.D., Welding Metallurgy and Weldability of Nickel-Base Alloys, John Wiley & Sons, 2009.

[10] Wang, N., Mokadem, S., Rappaz, M., Kurz, W., Solidification cracking of superalloy single- and bi-crystals. *Acta Mater.* 2004, *52*, 3173–3182.

[11] Rong, P., Wang, N., Wang, L., Yang, R.N., et al., The influence of grain boundary angle on the hot cracking of single crystal superalloy DD6. *J. Alloys Compd.* 2016, *676*, 181–186.

[12] Böllinghaus, T., Hot Cracking Phenomena in Welds, Springer-Verlag Berlin Heidelberg, Berlin/Heidelberg 2005.

[13] Osoba, L.O., A STUDY ON LASER WELDABILITY IMPROVEMENT OF NEWLY DEVELOPED HAYNES 282 SUPERALLOY, The University of Manitoba, 2012.

[14] Wilken, K., Kleistner, H., The classification and evaluation of hot cracking tests for weldments. *Weld. World* 1990, *28:7*, 126–143.

[15] Feng, Z., et al., Thermal Stress Development in a Nickel Based Superalloy During Weldability Test. *Weld. J.* 1997, *76:11*, 470–483.

[16] Feng, Z., et al., Modeling of Thermomechanical Conditions in the Sigmajig Weldability Test, in: *Trends in Welding Research*, Proceedings of the 4th International Conference, 5-8 June, Gatlinburg, Tennesee 1995, pp. 621–626.

[17] J. Lippold et al., Sigmajig weldability testing: The effect of specimen strength and thickness on cracking susceptibility. *EWI Rep. No. MR9401* 1994.

[18] B. Seth et al., Superalloys with improved weldability for high temperature applications, US Patent No. 6,284,392 B1, 2001.

[19] Birch, S., Pargeter, R., Effect of composition and laser focus position on solidification cracking susceptibility in C-Mn steel CO2 laser welds. *TWI Rep. No. MR755* 2002.

[20] G. Rees, Compositional factors controlling solidification cracking in C-Mn steel laser welds. *TWI Rep. No. MR623* 1997.

[21] SIS-CEN ISO/TR 17641-3, Destructive tests on welds in metallic materials – Hot cracking tests for weldments – Arc welding processes – Part 3: Externally loaded tests. 2005.

[22] Organizations, E.W.I.M., Comparison of Weld Hot Cracking Tests Summary of an IIW Round Robin Study. 2002, 27.

[23] Lundin, C.D., Lingenfelter, A.C., Grotke, G.E., Lessmann, G.C., et al., WRC Bulletin 1982 The varestraint test. *Weld. Res. Counc. - Bull.* 1982, *280*, 19.

[24] Organizations, E.W.I.M., Standardization of the Transvarestraint Test : A Statistical Study using Austenitic Stainless Steels and Nickel-Base Alloys. 2004.

[25] Z.sun, A study of solidification crack susceptibility usung the solidification cycle hot-tension test. *Mater. Sci. Enginering* 1992, *A151:1*, 85–92.

[26] Wilken, K., Investigation to Compare Hot Cracking Tests -Externally Loaded Specimen-. *Ger. IIW-Doc. IX-1945-99* 1999.

[27] Thomas, B., Herold, H., Böllighaus, T., Herold, H., et al., Hot Cracking Phenomena in Welds II, Springer Berlin Heidelberg, Berlin, Heidelberg 2008.

[28] B. Alexandrov, et al., Development of a Weldability Test for High Performance Ni-Base Alloys. *EWI Rep. No. MR0606* 2006.

[29] Andersson, J., Weldability of Precipitation Hardening Superalloys – Influence of Microstructure, Chalmers University of Technology, 2011.

[30] Vishwakarma, K.R.R., Richards, N.L.L., Chaturvedi, M.C.C., Microstructural analysis of fusion and heat affected zones in electron beam welded ALLVAC® 718PLUS™ superalloy. *Mater. Sci. Eng. A* 2008, *480*, 517–528.

[31] Andersson, J., Sjöberg, G., Brederholm, A., Hänninen, H., Solidification cracking of Alloy Allvac 718Plus and Alloy 718 at transvarestraint testing. *EPD Congr. 2008, TMS, Ed. SM Howard* 2008, *3*, 13.

[32] Idowu, O. a. A., Ojo, O. a. A., Chaturvedi, M.C.C., Effect of heat input on heat affected zone cracking in laser welded ATI Allvac 718Plus superalloy. *Mater. Sci. Eng. A* 2007, *454–455*, 389–397.

[33] Vincent, R., Precipitation around welds in the nickel-base superalloy, Inconel 718. *Acta Metall.* 1985, *33*, 1205–1216.

[34] Andersson, J., Sjöberg, G., Viskari, L., Brederholm, A., et al., Hot cracking of Allvac 718Plus, Alloy 718 and Waspaloy at Varestraint testing. *Proc. 47th Conf. Metall.* 2008, 16.